Elshafei *et al.*
Journal of Engineering and Applied Science (2024) 71:159
https://doi.org/10.1186/s44147-024-00491-x

Journal of Engineering and Applied Science

RESEARCH Open Access

Experimental study on the behavior of small-scaled circular and square RC columns under various loading conditions and corrosion effect

Merna Elshafei[1], Hany Abdalla[1] and Ahmed Youssef[1*]

*Correspondence:
ahmedyoussef@cu.edu.eg

[1] Department of Structural Engineering, Faculty of Engineering, Cairo University, Giza, Egypt

Abstract

Reinforced concrete columns are vital load-bearing elements, responsible for transferring vertical loads and resisting lateral forces. While numerous factors govern column performance, this study pinpoints cross-sectional shape, transverse reinforcement configuration, and the corrosive threat as its primary areas of investigation. Thus, 20 small-scaled (1/8th scale) RC columns (square and circular, with ties or spirals) were tested under various loading conditions. Columns were divided into five groups. A preliminary test was conducted to determine individual axial load capacity through failure under axial compressive loading. The main test then explored their behavior under combined axial load and variable lateral drift compared to their behavior at two corrosion levels 15% and 25%. While corrosion levels were roughly achieved, uneven distribution due to the accelerated process concentrated pitting near construction joints, impacting reinforcement more than rebar. Results confirmed the efficacy of spirals in enhancing capacity, particularly for circular columns where they also increased lateral load capacity. However, spirals also amplified corrosion vulnerability in circular columns, suggesting a steeper decline in performance at higher corrosion levels. Two key models were derived from analyzing the recorded data: normalized total dissipated energy and normalized absolute peak load. Future research should prioritize exploring column behavior under a wider range of combined loads and corrosion levels to refine and validate these models.

Keywords: Square column, Circular column, Lateral drift, Accelerated corrosion, Small-scale specimens

Introduction

The performance of reinforced concrete columns is governed by a complex interplay of factors, including cross-sectional shape, transverse reinforcement configuration, and reinforcing steel corrosion. Circular sections offer superior flexural performance due to their uniform stress distribution, while square and rectangular sections require careful design considerations. Transverse reinforcement, in the form of ties or spirals, enhances

compressive strength, ductility, and shear resistance. Understanding the impact of corrosion on both steel and concrete is crucial for ensuring long-term structural durability.

This research aims to investigate the interactions between cross-sectional shape, transverse reinforcement configuration, and corrosion degradation in reinforced concrete columns. Specific objectives include quantifying the influence of cross-sectional shape on load-carrying capacity, ductility, and failure modes under various loading scenarios. Moreover, evaluating the effectiveness of ties versus spirals in enhancing column performance under combined axial and lateral varying drift. Furthermore, assessing the impact of corrosion on the structural behavior of columns with different shapes and transverse reinforcement types.

Understanding the long-term effects of steel corrosion on concrete structures is crucial for their safe and reliable operation. However, testing for durability under natural conditions can be time-consuming. Therefore, researchers use various accelerated corrosion methods to simulate and expedite the deterioration process. These methods typically involve one or a combination of three main principles: (1) applying an electrical current to the embedded steel (galvanostatic method), (2) exposing the samples to high humidity environments (through spraying, ponding, or wetting–drying cycles), and (3) introducing chlorides to the samples (either by adding them directly to the mixing water or by immersing the samples in a chloride solution).

Austin et al. [1] aimed to analyze and evaluate the method of using impressed current to speed up chloride-induced corrosion and also to examine the electrochemical implications of applying an external current and compare it to the natural electrochemistry of steel reinforcement (RFT) corrosion. It was found that the impressed current method has been validated as a successful and expedient approach to accelerate chloride-induced corrosion. However, the electrochemical principles underlying this mechanism differ from naturally occurring corrosion. Moreover, the thickness of the concrete cover exerted a more significant influence than the strength of the concrete in determining the time required for chlorides to permeate through the cover.

Meda et al. [2] carried out preliminary tests on bare and embedded bars for the calibration and optimization of the artificial corrosion process. Faraday's law was used to estimate the time needed to obtain the desired corrosion level; a modification was suggested to take the presence of concrete into consideration, the required time is multiplied by a constant taking into consideration the likelihood that the corrosive process would not begin right away.

Li et al. [3] investigated the influence of various wiring methods on the characteristics of artificially induced corrosion in longitudinal reinforcement and stirrups of concrete specimens. Their objective was to assess the applicability of accelerated corrosion techniques. The study concluded that the employed wiring method, regardless of its type, did not affect the distribution patterns of cracks caused by rust expansion or the color of rust leakage on the specimen surfaces under identical corrosion conditions.

Basdeki et al. [4] explored the nonlinear behavior of corroded reinforced concrete (RC) specimens under two corrosion scenarios: uniform and pitting. Their findings revealed that when corrosion damage remained low, with a mass loss of up to 6% in the steel reinforcement, the corrosion pattern was uniform. However, at higher corrosion levels exceeding 6% mass loss, the corrosion transitioned to pitting, characterized

by the formation of localized deep cavities on the steel surface. This pitting corrosion resulted in stress concentrations around the pits, fundamentally altering the behavior of the corroded columns. These changes manifested as a propensity for rapid failure under dynamic loading conditions.

Li et al. [5] conducted experiments to investigate the behavior of short concrete columns with corroded stirrups [5]. Their findings indicated that corrosion in the stirrups progressed unevenly throughout the concrete specimens. This uneven corrosion resulted in the expansion of corrosion products, which in turn caused partial or complete failure of the concrete cover. Consequently, the effective cross-sectional area of the reinforced concrete (RC) short columns was reduced. This reduction in stiffness triggered a critical shift in the failure mode, transitioning from ductile failure (where the column can deform significantly before breaking) to brittle failure (where the column breaks with minimal deformation) as the specimens deteriorated.

Meda et al. [2] investigated the change of the collapse mechanism caused by decreased structural ductility due to corrosion in main steel only. Test results revealed that the corroded column suffered a reduction in both ultimate force and ultimate displacement and also sharp stiffness degradation in the last two cycles compared to the uncorroded column.

Mohammed et al. [6], Ahmed et al. [7], Mohammed et al. [8], Mohammed et al. [9], Ahmed et al. [10], and Ahmed et al. [11] experimentally and analytically investigated the behavior of corroded tied columns under simulated seismic loads. It was found that the higher the corrosion ratio was, the lower the cracking load became. Also, the higher the axial compression ratio was, the higher the cracking load became. Considering the ductility ratio, the corrosion of steel bars enhances the ductility of the specimen but diminishes its ability to dissipate seismic energy. Moreover, crack width became wider for specimens with higher corrosion level.

Spiral reinforcement's influence on corrosion cracking patterns was also explored. Experimental tests by Jabbour and Martín-Pérez [12] revealed that columns with corroded longitudinal reinforcement exhibited vertical cracks parallel to the reinforcing bars. On the other hand, columns with corroded spiral reinforcement displayed a more random cracking pattern distributed laterally. Overall, columns with corroded longitudinal reinforcement experienced higher axial and lateral deformations compared to those with corroded spiral reinforcement. Additionally, the crack widths associated with corrosion in the longitudinal reinforcement were six to eight times greater.

Ma et al. [13] investigated the corroded column behavior under axial load combined with seismic load. It was found that for the same axial load ratio, but in highly corrosion-damaged specimens, less stable hysteretic loops with smaller hysteretic loop areas. At the same time, the higher axial load ratio may cause the corroded specimens' capacity to dissipate energy and ductility to decrease even further, and for the severely damaged columns with corrosion loss ratios between 10 and 20% exhibited poor hysteretic response, stiffness degradation, a steep descending branch in the envelop curve, ductility loss, and a decrease in energy dissipation.

Several studies support the detrimental effect of corrosion on the axial capacity of spirally reinforced concrete columns (Radhi et al. [14], Jabbour et al. [15] and Mahmood & Lateef [16]). These studies consistently report a significant decrease in axial load

capacity and final displacement as the corrosion level increases. Additionally, corrosion negatively affects the stiffness and ductility of the columns, reflected in a reduction of the stress–strain curve's slope. Furthermore, a critical finding is the influence of corrosion on the failure mode. As the corrosion level progresses, the failure mode transitions from shear failure to splitting and debonding, highlighting a more critical degradation mechanism.

Extensive research has investigated the behavior of corroded reinforced concrete columns under various loading conditions, considering a range of cross-sectional geometries including rectangular, square, and circular shapes.

Saeedi Razavi et al. [17] investigated the effect of transverse reinforcements corrosion on axial strength of circular and square spirally reinforced columns. It was found that reduction in strength of the spirally reinforced circular columns is greater than that of the square columns confined by stirrups. Which proves that spirals are more prone to corrosion than stirrups.

Aminulai et al. [18] studied the behavior of corroded reinforced concrete columns subjected to cyclic axial compressive load. The comparison between circular and square RC columns revealed that the ultimate strain-to-strength ratio of circular reinforced concrete columns generally exceeded that of their square counterparts, excepting situations with minimal confinement. While both experienced a downward trend in energy dissipation with increasing corrosion and confinement, square columns suffered a more pronounced decline due to their inherently less effective confinement mechanisms.

This research examined the combined effects of cross-sectional shape (square, circular), transverse reinforcement configuration (ties vs spirals), and corrosion on the behavior of reinforced concrete columns under various loading conditions. To achieve this, 20 small-scale column specimens were cast and divided into 5 groups. Each group underwent a series of tests, allowing for both comparative studies to understand the influence of cross section shape and corrosion, and individual comparisons across cross section shapes and reinforcement configurations to isolate the impact of corrosion. By analyzing the total energy dissipated by the columns during testing, two key models were developed for each column type: a normalized model for total dissipated energy and a normalized model for the peak load experienced. These models provide valuable insights into the behavior of columns under these combined factors.

Methods

The experiment utilized a structured approach, dividing the research into five distinct groups, each comprising four individual specimens. Consequently, each group contained four specimens representing the combinations of these variables: square tied, square spiral, circular tied, and circular spiral. Employing manually operated load cell tests, this research conducted small-scale (1:8) mortar column experiments to explore the multifaceted interplay between cross-sectional geometry, transverse reinforcement configuration, and the effects of corrosion in reinforced concrete columns. The research evaluated the relative efficacy of ties and spirals in enhancing column performance under combined axial and variable lateral drift loading. Limited availability of resources necessitated selectively energizing the rebar specimens during corrosion testing, but the carefully designed specimens enabled systematic investigation of several key variables:

cross-sectional shape, transverse reinforcement configurations, and the impact of corrosion on the structural behavior of columns with varying geometries and reinforcement types. This comprehensive approach delves deep into the complex interactions governing reinforced concrete column performance, providing valuable insights for real-world engineering applications.

Test setup

The experimental investigation took place within the Concrete Research Laboratory at Cairo University. Prior to the main experiment, a preliminary test was conducted to establish the axial load capacity of various column cross-sectional shapes. The main test is designed to explore the behavior of these different shapes under the combined action of constant axial load and variable horizontal drift compared to two levels of corrosion.

The objective of the preliminary test was to obtain the axial load capacity of each specimen. Hence, all specimens were loaded axially till failure while single LVDT was used to measure specimen's shortening. It is worth mentioning that steel encasement was used to prevent premature bearing failure. Figure 1a shows the schematic of the axial compressive load test setup. Meanwhile, Fig. 1b shows the actual test setup.

To assess the initial axial load capacity, a preliminary test was conducted before the main experiment. Specimen naming for Group 1 followed a simple convention: "X–Y," where "X" denoted the cross-sectional shape ("Sq" for square, "C" for circular) and "Y" signified the transverse reinforcement type ("T" for tied, "Sp" for spiral).

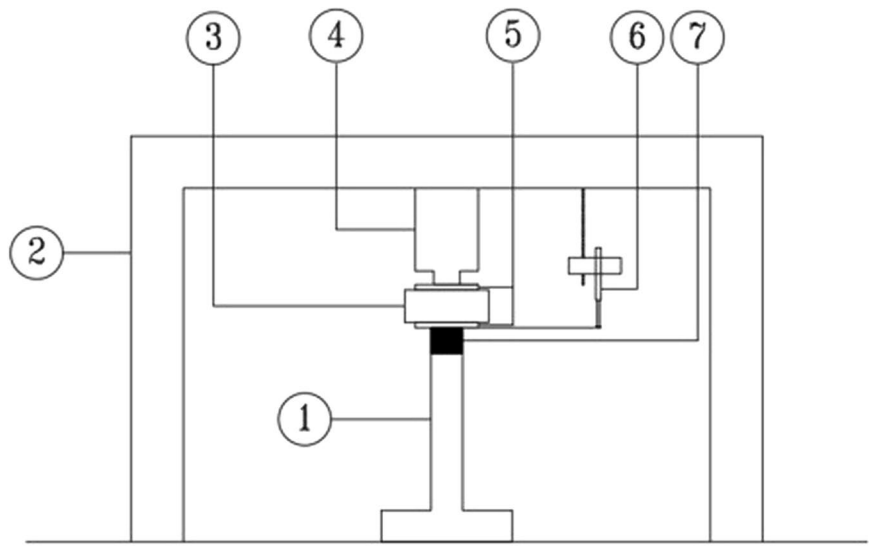

Fig. 1 Axial compressive load test setup

Subsequent groups differed in their loading regime. Group 2 specimens were subjected to a constant axial load (100 kN) combined with varying horizontal drift, while groups 3–5 experienced a constant axial load ratio (40% of reference capacity) with varying drift. Hence, these groups adopted a more elaborate naming scheme: "X-Y-A-B," where "A" indicated the axial load ratio as a fraction of reference capacity and "B" represented the corrosion level, as illustrated in Table 1.

Within the main test, the specimen was secured to the table with four bolts; to minimize friction effect, the column's loading face was pre-treated with a thin layer of grease. Subsequently, the axial compressive load was applied with the specimen's geometric center aligned with the vertical load, followed by the lateral drift sequence. Throughout the experiment, precise measurements were recorded for horizontal and axial forces, top and bottom lateral drift of the column, and any potential slippage at the footing.

Figure 2 depicts the schematic for horizontal varying drift test setup and instructions used in the study.

Previous research has proved that the utilized wiring method has minimal impact on the current flow (Q. Li et al. [3]). Therefore, prior to casting the column, a single wire connected to the longitudinal rebars was adopted in this study. The footing was encased in an insulating plastic barrier to restrict the flow of current into the footing's reinforcement and to keep the electricity focused on the column's steel cage flowing radially targeting only column's reinforcing steel. The concrete column was prepared for the accelerated corrosion process by enveloping it in a layer of sponge designed to retain the required 5% saline solution. This sponge layer was then further encased within a steel mesh, acting as the cathode. Moreover, to maintain the desired level of

Table 1 Specimen group test details

Group	Specimen type	Code	Test	Corrosion
1	Square tied	Sq-T	Axial compression load till failure	Nil
	Square spiral	Sq-Sp		
	Circular tied	C-T		
	Circular spiral	C-Sp		
2	Square tied	Sq-T-95-0	Constant axial compression load and varying lateral drift (axial compression load = 100 kN)	Nil
	Square spiral	Sq-Sp-81-0		
	Circular tied	C-T-91-0		
	Circular spiral	C-Sp-76-0		
3	Square tied	S-T-40-0	Constant axial compression load and varying lateral drift (Axial compression load = 40% of reference column capacity)	Nil
	Square spiral	Sq-Sp-40-0		
	Circular tied	C-T-40-0		
	Circular spiral	C- Sp-40-0		
4	Square tied	S-T-40-15		15%
	Square spiral	Sq-Sp-40-15		
	Circular tied	C-T-40-15		
	Circular spiral	C- Sp-40-15		
5	Square tied	S-T-40-25		25%
	Square spiral	Sq-Sp-40-25		
	Circular tied	C-T-40-25		
	Circular spiral	C- Sp-40-25		

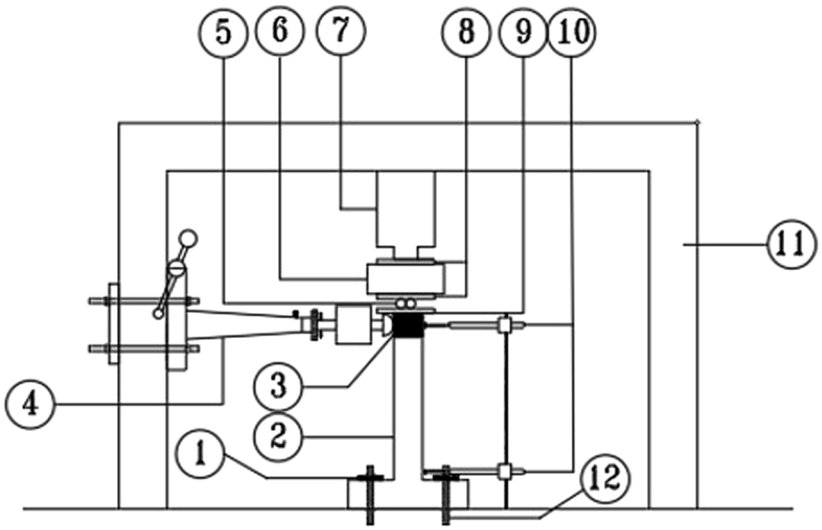

1: Steel plate 2: Specimen 3: Steel encasement
4: Manual hydraulic jack 5: Roller 6: Load cell
7: Hydraulic jack 8: Steel plates 9: Grease layer
10: LVDTs 11: Steel frame 12: Fixed bolts

(a): Schematic for main test setup.

(b) Main test setup.

Fig. 2 Main test setup. **a** Schematic for main test setup. **b** Main test setup

moisture for the accelerated corrosion process, the steel mesh was carefully wrapped in a non-porous plastic material, thereby ensuring the retention of the 5% saline solution. Figure 3 illustrates the schematic of accelerated corrosion setup.

The specific duration needed to reach particular corrosion percentages was subsequently determined using Equation 1.

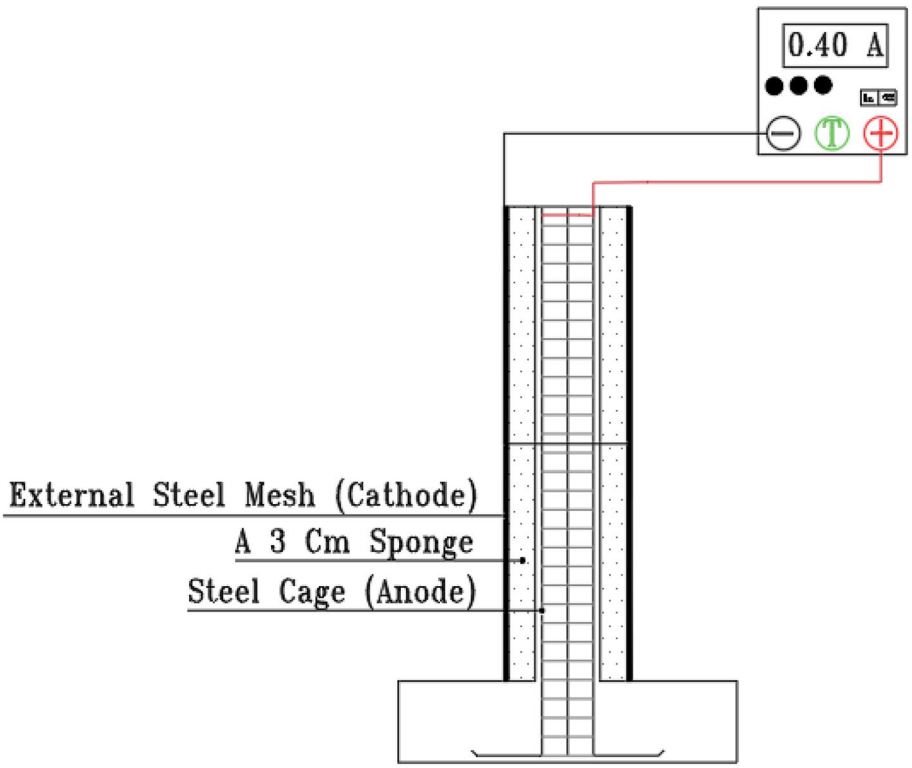

Fig. 3 Schematic of accelerated corrosion setup

$$\text{Time} = \frac{\lambda.n_{\text{specimen}}.C_{\text{Faraday}}.m_{\text{loss}}}{\text{current}.M_{\text{specimen}}} * \frac{1}{3600} = \frac{1.3 * 2 * 96{,}485 * m_{\text{loss}}}{\text{current}.55.8} * \frac{1}{3600}(h) \quad (1)$$

To investigate the impact of corrosion level, eight concrete specimens were cast, divided into two groups representing two different corrosion levels. Each group was then subjected to a series of tests that combined vertical loading with lateral drift of varying magnitudes. To validate Equation 1, the weight of the steel reinforcement in each specimen was precisely measured before casting and after testing as illustrated in Table 2.

Cross section selection and reinforcement details

The specimens' dimensions were made from a designed column dimensions with a scale down of one eighth. To provide a comparable reference point, a square column with an identical cross-sectional area was selected. The material of the formwork differed. Where wood served as the material of choice for constructing the formwork for both the footing and square columns. In contrast, plastic pipes were chosen for the formwork of circular columns. To facilitate effortless demolding and enable mold reuse, the plastic pipes were cut along their length. This pre-cutting ensures smooth removal of concrete samples after casting. Section reinforcement arrangement of square specimens and circular specimens are illustrated in Fig. 4.

Table 2 Corrosion specimens' details

Specimen's name	Targeted corr. level (%)	RFT weight before corrosion (g)		RFT weight after corrosion (g)		Actual corrosion (%)			Actual time of corr. (day)
		Longitudinal RFT	Transverse RFT	Longitudinal RFT	Transverse RFT	Longitudinal RFT	Transverse RFT	Total	
Sq-T-40-15	15	235	160	203	135	11.7	15.63	13.3	7
Sq-Sp-40-15	15	247	123	205	117	14.9	15.2	15	7
C-T-40-15	15	236	155	208	134	11.56	13.55	12.5	7
C-Sp-40-15	15	213	130	208	113	15.1	16.15	15.47	7
Sq-T-40-25	25	255	155	198	113	22.3	27.1	24.15	12
Sq-Sp-40-25	25	235	160	195	98	17	38.75	25.8	12
C-T-40-25	25	236	155	182	115	22.9	25.8	24	12
C-Sp-40-25	25	262	133	190	69	22.9	25.8	24.5	12

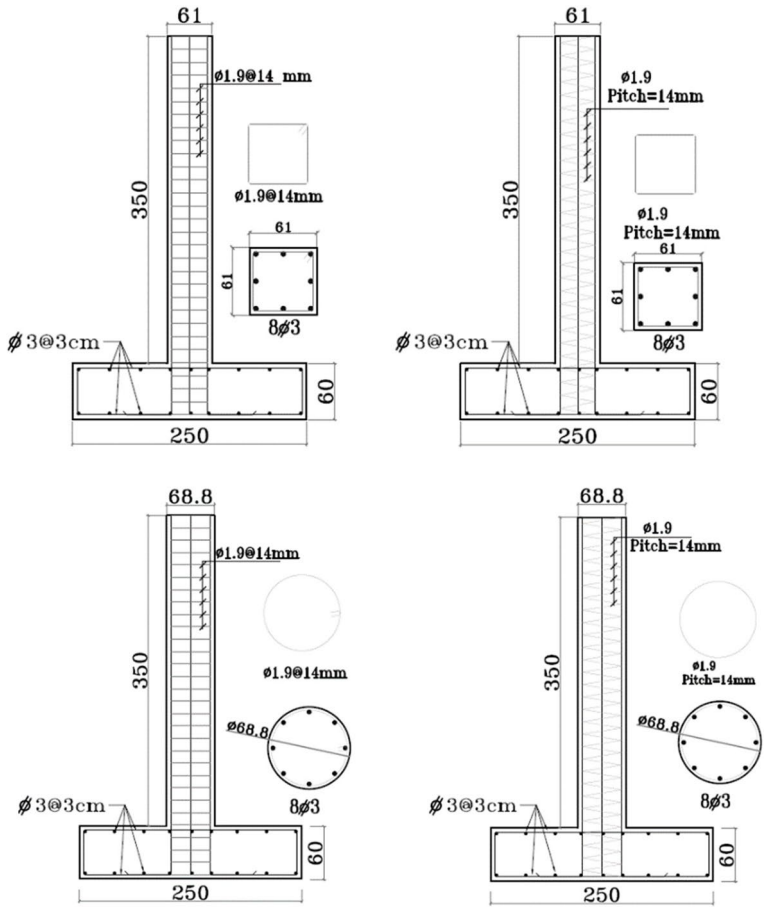

Fig. 4 Section reinforcement arrangement specimens

Casting procedure

Following numerous unsuccessful casting attempts, the study adopted the preferred technique of separate casting, pouring the footing first and allowing it to set before proceeding with the column. To facilitate easy removal of the formwork after concrete setting, the wooden surfaces were pre-treated with a thin layer of oil, preventing unwanted adhesion. The initial stage involved constructing the specimen's footing and permitting the concrete to solidify for 1 day. Upon reaching adequate strength, the footing's formwork was removed and utilized for the following batch. The columns were then cast, precisely aligned for complete verticality and perfectly level loading surfaces. After a day of setting, the column's formwork was carefully removed and repurposed for efficiency in subsequent castings. Simultaneously, the concrete column entered curing stage, designed to maximize its strength and durability. This method, despite being less favorable, enjoys widespread adoption at local sites due to its familiarity and prevalence.

Material properties

This study employs readily available materials to enhance the applicability of its findings. Locally sourced clean sand, ordinary Portland cement (CEMI), and Addicrete BV

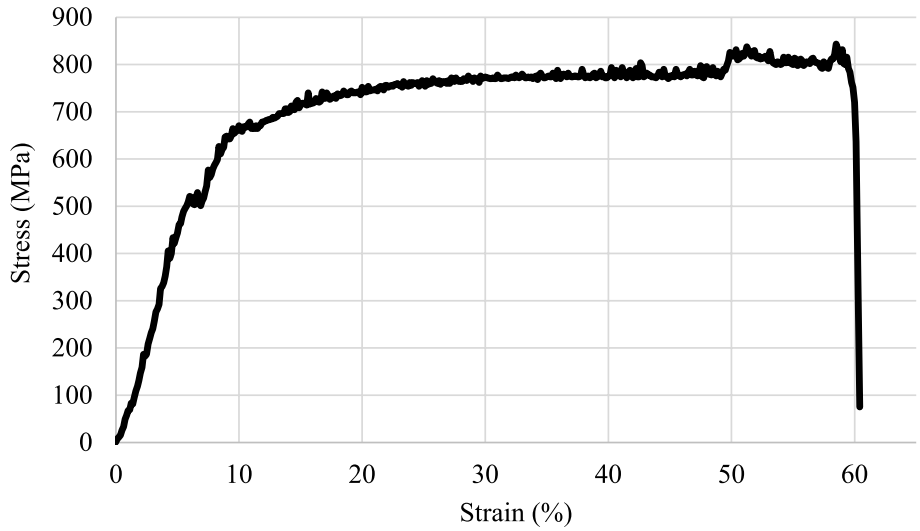

Fig. 5 Stress–strain curve for bar diameter (1.9 mm)

superplasticizer ensure feasibility and cost-effectiveness, where fine aggregate met strict cleanliness and size requirements (max. 4.75 mm) for minimal contamination. CEMI cement guaranteed a minimum 28-day strength of 42.5 MPa, ensuring structural integrity. Clean, potable water adheres to established quality standards for optimal hydration. Addicrete BV (0.005 g/L) improves workability, reduces water content, and accelerates early strength gain. Thus, 20 mortar cubes of $75 \times 75 \times 75$ mm were cast and tested in compression. Cubes were divided into four batches, each batch contained five cubes.

To ensure appropriate reinforcement characteristics, this study utilized two different grades of steel. The larger 3 mm diameter bars were chosen for the longitudinal reinforcement within the columns and the reinforcement steel in the footing, while the smaller 1.9 mm diameter bars provided the stirrups within the columns. Both sets of bars underwent tensile strength testing according to ECP-203 to verify their mechanical properties. Stress–strain curves for 1.9 mm and 3 mm steel are illustrated in Figs. 5 and 6, respectively. Table 3 shows the tensile test results.

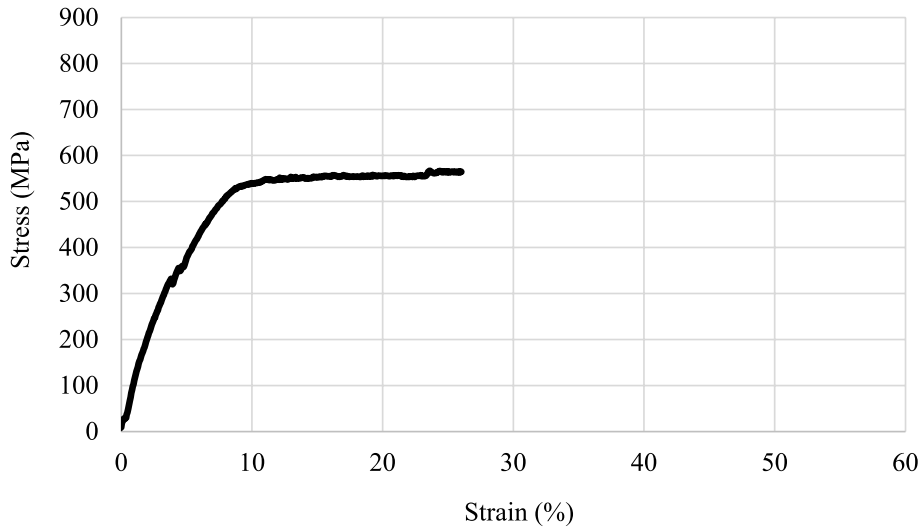

Fig. 6 Stress–strain curve for bar diameter (3.0 mm)

Table 3 The engineering mechanical properties of rebar reinforcement

Steel diameter (mm)	Yield point (N/mm^2)	Tensile strength (N/mm^2)
3	400	566.8
1.9	521.1	843.5

This research carefully selected mortar mix proportions based on desired properties and application objectives. Ratios of components by weight are carefully chosen considering factors like durability, strength demands, environmental impact, and application methods. Adherence to standardized guidelines or specifications for specific applications was essential to ensure the mortar met the required standards. Prior to specimen pouring, tests confirmed adherence to these criteria. Table 3 specifies the final ingredients employed across all specimen groups, while Table 4 showcases the actual compressive strength achieved during specimen pouring, further emphasizing the commitment to material selection and execution. It is also worth noting that average f_{cu} for all cubes was found to be 36.5 MPa.

A crucial consideration when employing small-scale reinforced concrete (RC) specimens for testing purposes is the shear size effect. This phenomenon dictates that larger concrete members exhibit a reduced shear strength per unit area compared to their smaller counterparts. To mitigate this discrepancy between the small-scale specimens and the actual concrete structures they represent, researchers frequently utilize a mortar mix devoid of coarse aggregate. The absence of these larger aggregate particles minimizes the influence of the shear size effect on the observed shear behavior within the specimens.

Furthermore, the use of coarse aggregate in very small molds for scaled models can present practical challenges. Due to the size disparity, casting and compaction of the concrete mix can become difficult. To address this limitation, the current investigation employed a mix without coarse aggregate for the small-scale specimens.

It is important to note that the absence of coarse aggregate, while mitigating the shear size effect, also leads to a denser and less porous mixture. This denser structure might seem counterintuitive, but it actually hinders the penetration and propagation of corrosion within the element. Consequently, we might expect a higher rate of localized and potentially more aggressive corrosion in the specimens with coarse aggregate. This is because the presence of voids in the concrete acts as a reservoir for the corrosive solution (salted water or electrolyte). A higher volume of such voids allows for a greater flow of the corrosion current, ultimately leading to more severe corrosion damage to the reinforcing steel.

Loading procedure and measurement

Specimens in Group 1 were tested under axial compressive load till failure. However, in Groups 2–5, a constant axial compressive load was applied. Subsequently, one-way

Table 4 Specimens of mortar final ingredients by weight

Sand (kg)	Cement (kg)	Water (kg)	Additives ADDICRETE BV (g/l of mixing water)	W/C
1000	600	240	0.005	0.40

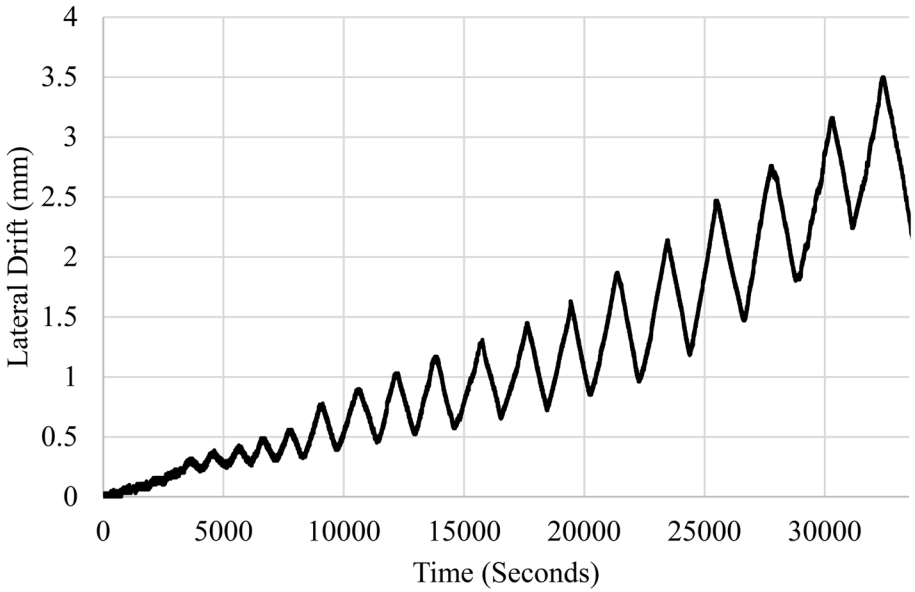

Fig. 7 Lateral drift versus time along the same specimen

varying gradually increasing drift was applied using the manual load cell at the top of the column. It is also worth mentioning that drift of the first cycle was 0.2 mm then increased by 0.2 mm up to total drift of 10 mm, then the drift increased by 2 mm up to failure. Following the lateral drift history is shown in Fig. 7. Group 2 was axially loaded with a constant value of 100 kN for all specimens. However, due to unpromising results, the axial load was modified for Groups 3–5 to be 40% of the reference specimen's capacity. It is also worth mentioning that specimen's failure was declared when the peak load of a cycle reached 60% of the ultimate peak load.

Results and discussion

Experimental observations documented the failure mechanisms exhibited by all specimens. For Group 1, axial load-shortening curves reveal the behavior of each type of columns and their axial compressive capacity. For Groups 2 through 5, the results included the relation between the lateral load and the corresponding drift. Furthermore, comparative studies are implemented to comprehend the influence of both cross-sectional shape and corrosion. Specifically, Group 1 focuses on examining the load-carrying capacity and maximum shortening, while Groups 2 to 5 utilize comparisons of group envelopes to elucidate the shape effect. Additionally, individual comparisons are made across all cross-sectional shapes and transverse reinforcement configurations to investigate the impact of corrosion. After analyzing the total dissipated energy and its variations, based on the results, two key models for each column type were derived: a normalized total dissipated energy model and normalized absolute peak load model.

Result of axial compressive load test

Both tied and spiral columns exhibited distinct failure mechanisms under axial compressive load as shown in Fig. 8. Tied columns suffered sudden and localized buckling

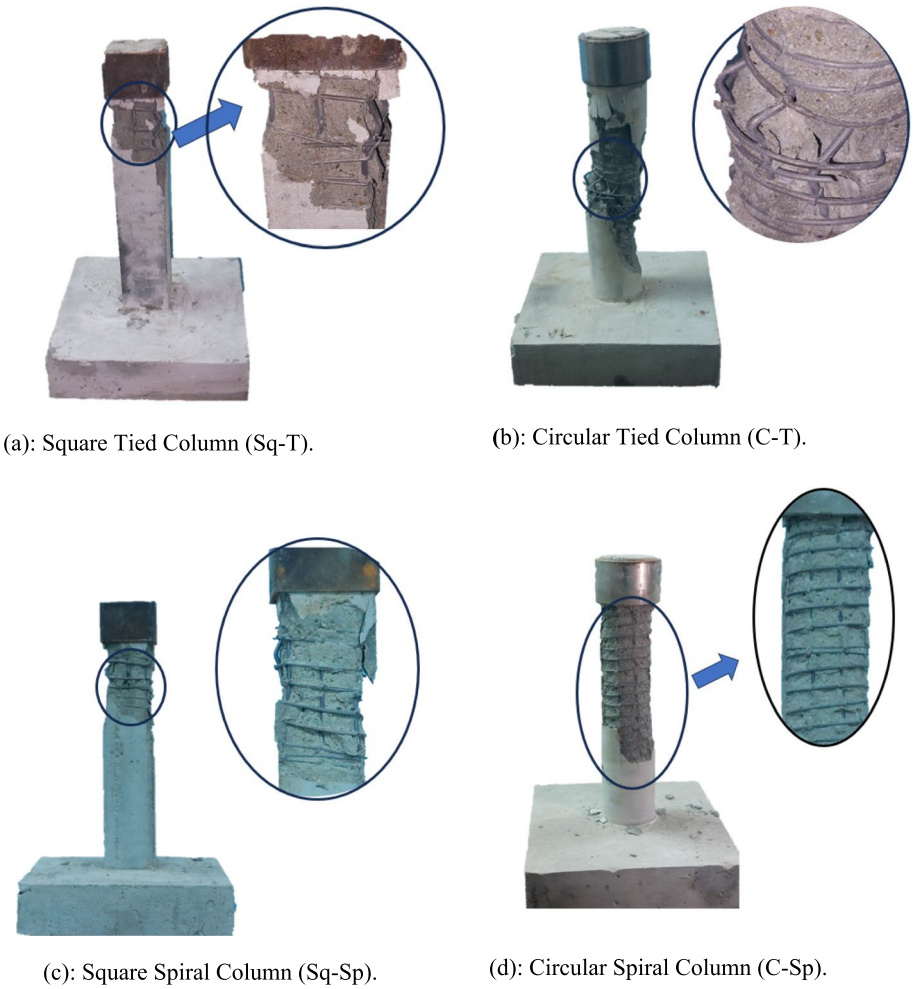

Fig. 8 The failure mode of Group 1 specimens. **a** Square tied column (Sq-T). **b** Circular tied column (C-T). **c** Square spiral column (Sq-Sp). **d** Circular spiral column (C-Sp)

of longitudinal reinforcement, with the failure location varying square columns failing near the steel encasement due to wider tie spacing, and circular columns failing in the mid-height region. In contrast, spiral columns provided a warning sign through progressive concrete cover crushing before ultimate failure. This distributed crushing across a larger area allowed the reinforced core to retain load-carrying capacity despite significant damage.

Transverse reinforcement type significantly influenced the load-carrying capacity of concrete columns as shown in Fig. 9 which revealed that using spiral instead of stirrups increased the load-carrying capacity by 16.13% and 20% for square and circular columns respectively. Meanwhile, final shortening, a measure of axial deformation, was also significantly affected by the type of transverse reinforcement. Hence, square sections displayed a 53.2% increase in final shortening with spiral reinforcement compared to tied reinforcement. Likewise, circular sections demonstrated a 32% increase in deformation with spiral reinforcement. This underscores the enhanced ductility associated with spiral reinforcement, allowing for larger deformations before failure.

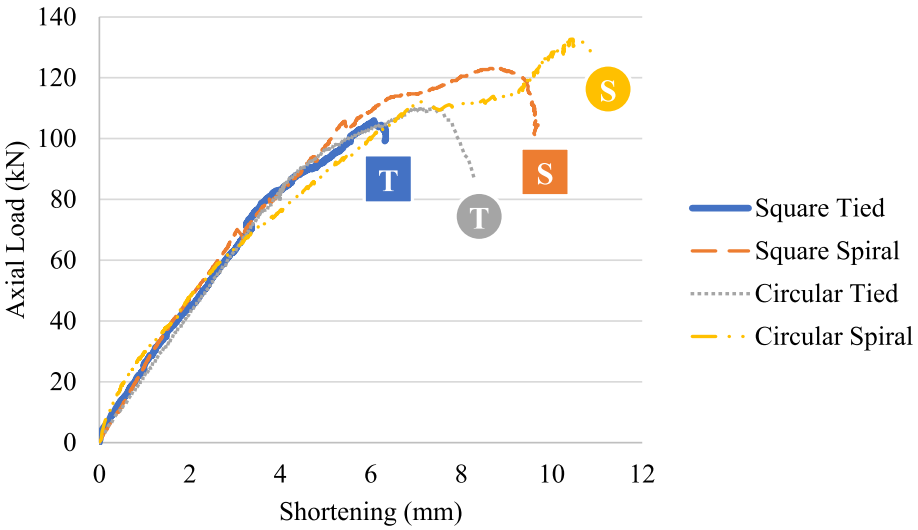

Fig. 9 The axial load-shortening curve for axial compressive loaded specimens

Comparative analysis of tied and spiral reinforcement in square and circular columns reveals interesting cross-sectional effects. Replacing the circular cross-section with a square in tied columns resulted in a 4.3% reduction in load-carrying capacity and a significant 31.2% decrease in final shortening. This trend continued for spiral columns, where switching to a square section led to a 7.8% drop in load capacity and a less pronounced 13% decrease in final shortening. These findings suggest that circular sections are generally more effective in maximizing both strength and ductility for both tied and spiral reinforcement configurations.

Result of non-corroded specimens

To replicate the influence of real-world forces encountered in structures, the specimen underwent cyclic horizontal loading throughout the test. These forces can originate from construction activities (vertical loads) and seismic events (earthquakes). Table 5 shows horizontal cyclic loading specimens failure mode commentary.

For Group 2, a constant axial compressive load of 100 kN was applied first using the hydraulic jack to simulate the load on column. Subsequently, one-way varying gradually increasing drift was applied using the manual load cell at the top of the column. Figure 10 shows the failure mode of Group 2 specimens; however, Fig. 11 shows the horizontal load versus lateral drift curves.

Comparative analysis of tied concrete columns reveals a significant influence of cross-sectional shape on horizontal load and lateral drift as depicted in Fig. 12. Circular tied columns exhibited a 13.46% *reduction* in absolute horizontal peak load and a 28% *increase* in maximum lateral drift compared to their square counterparts. Similarly, for square columns, replacing tied separate stirrups with spiral reinforcement resulted in a 21.14% *decrease* in absolute horizontal peak load and a 13% *increase* in maximum lateral drift. Additionally, variations in axial load ratio directly impacted the absolute horizontal

Table 5 Horizontal cyclic loading specimens failure mode commentary

Group no	Commentary
Group 2	Most of the specimens displayed a consistent failure pattern characterized by horizontal cracks on the side facing the load and crushing of the concrete cover on the opposite side, indicative of bending-dominant failure as shown in Fig. 10b, c. Some specimens exhibited additional localized damage like cracks and cover crushing near the top encasement, likely due to stress concentrations arising from the encasement intended to prevent bearing failure as depicted in Fig. 10a. However, specimen C-Sp-76-0 deviated due to its susceptibility to axial compression, exhibiting focused concrete cover crushing along the middle third of its height as illustrated in Fig. 10d.
Group 3	The majority of tested specimens displayed a consistent failure mode characterized by horizontal cracks on the load-facing side and concrete cover crushing on the opposite side as shown in Fig. 13a, d. This widespread pattern indicates a bending-dominated failure mechanism, where bending stresses were the primary contributor to failure. While most specimens exhibited this behavior, some showed additional localized damage in the form of cracks and cover crushing near the top encasement as depicted in Fig. 13b, c. This localized damage is likely due to stress concentrations caused by the encasement, which was implemented to prevent bearing failure at the column top.

peak load, with higher ratios leading to larger horizontal loads until reaching the critical point of failure due to axial compression only as occurred in specimen C-Sp-76-0.

To ensure fair comparisons across different test groups, the research adopted a normalized axial load approach. This involved setting the axial load for Groups 3–5 at 40% of the individual specimen's capacity (from Group 1). This eliminated the influence of inherent capacity variations between specimens, leading to more reliable and generalizable observations on column behavior.

In practical terms, this translated to a constant load of 40 kN for all tied columns and 60 kN for all spirally reinforced columns throughout the experiment. Figure 13 depicts the failure mode observed in the control reference specimens (Group 3). Figure 14 represents the horizontal load- lateral drift curves for Group 3. Figure 15 shows the comparison of the envelopes for Group 3.

Notably, circular tied columns exhibited an 18% increase in absolute horizontal peak load and a 21.5% decrease in maximum lateral drift compared to square tied columns. Similarly, replacing squares with circles in spiral columns increased the absolute horizontal peak load by 26% and reduced the maximum lateral drift by 15%. Within each

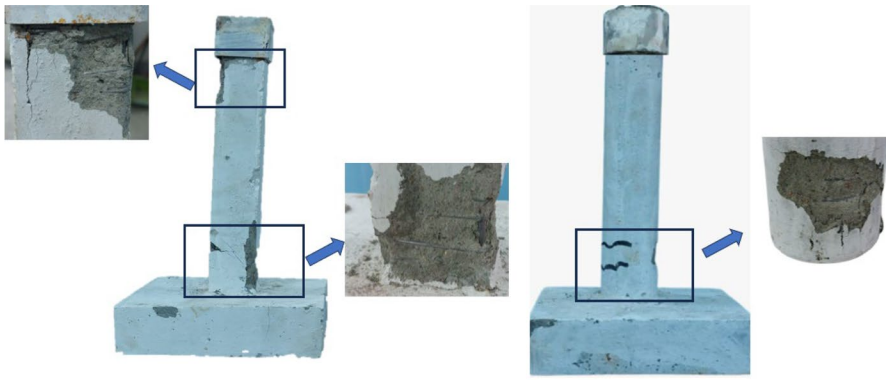

(a): Square Tied Column (Sq-T-95-0). (b): Circular Tied Column (C-T-91-0).

(c): Square Spiral Column (Sq-Sp-81-0). (d): Circular Spiral Column (C-Sp-76-0).

Fig. 10 The failure mode of Group 2 specimens. **a** Square tied column (Sq-T-95-0). **b** Circular tied column (C-T-91-0). **c** Square spiral column (Sq-Sp-81-0). **d** Circular spiral column (C-Sp-76-0)

shape, spiral reinforcement significantly enhanced load-carrying capacity, with square and circular sections experiencing increases of 32% and 40.86%, respectively. However, the impact on drift differed, with squares showing a 5.27% decrease and circles a modest 2.44% increase in maximum lateral drift.

Result of rebar reinforcement corrosion effect

Groups 4 and 5 underwent accelerated degradation processes to simulate the effects of real-world corrosion. Group 4 specimens were exposed to a constant electric current of 0.4 Amps for 7 days, targeting a predetermined mass loss of 15%. Similarly, Group 5 specimens were exposed to the same current for 12 days to achieve a 25% mass loss. Following this simulated corrosion, both groups were tested using the identical testing protocol employed for Group 3. The failure modes, horizontal load-lateral drift, envelope curved observed in Groups 4 and 5 are illustrated in Figs. 16, 17, 18, 19, 20 and 21, respectively. Table 6 shows the results commentary of failure mode of corroded specimens.

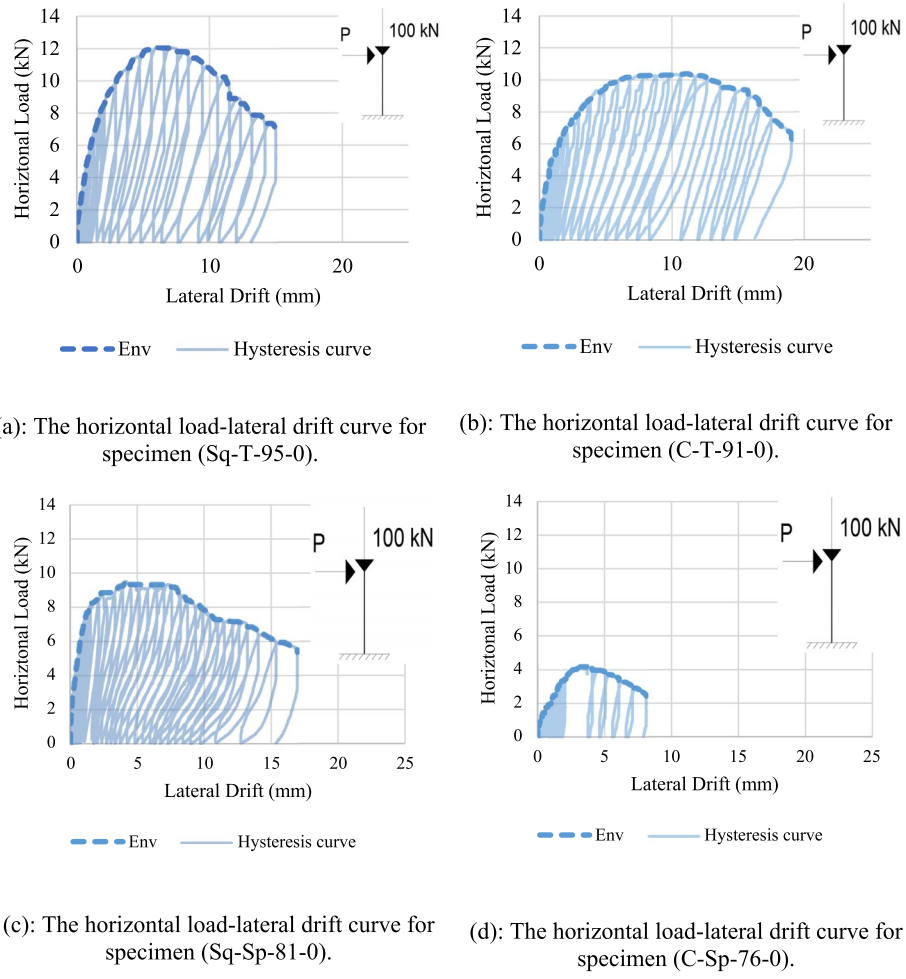

Fig. 11 The horizontal load-lateral drift curve for Group 2. **a** The horizontal load-lateral drift curve for specimen (Sq-T-95-0). **b** The horizontal load-lateral drift curve for specimen (C-T-91-0). **c** The horizontal load-lateral drift curve for specimen (Sq-Sp-81-0). **d** The horizontal load-lateral drift curve for specimen (C-Sp-76-0)

Comparative analysis of tied and spiral reinforced concrete columns reveals a complex interplay between cross-sectional shape and transverse reinforcement configuration at 15% corrosion level as depicted in Fig. 18. Comparing tied columns, circular column exhibited a 21.74% increase in absolute horizontal peak load compared to square column, accompanied by a 16.3% decrease in maximum lateral drift. This suggests that circular sections offer superior load-carrying capacity but at the cost of reduced ductility. While the difference in absolute horizontal peak load between circular and square spirally reinforced columns was smaller. Where the circular column increased the absolute horizontal peak load by 20%. However, the impact on maximum lateral drift was reversed. Circular column displayed a 7.8% increase in maximum lateral drift, indicating enhanced ductility despite slightly lower strength compared to square column.

Replacing tied stirrups with spirals led to significant increases in the absolute horizontal peak load (30.71% for square, 28.8% for circular). This highlights the effectiveness of spiral reinforcement in enhancing the load-carrying capacity of concrete columns. Meanwhile, for square column, spiral reinforcement was associated with a decrease in

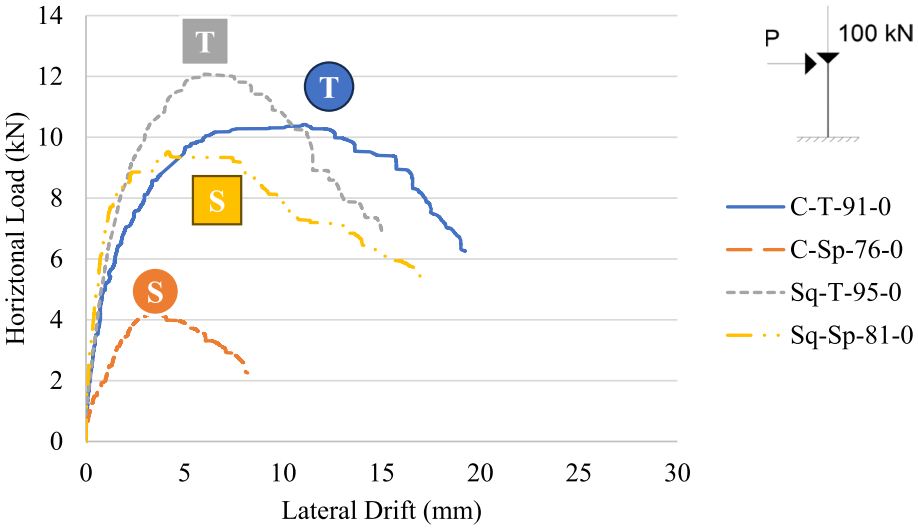

Fig. 12 Envelope curves for Group 2 specimens

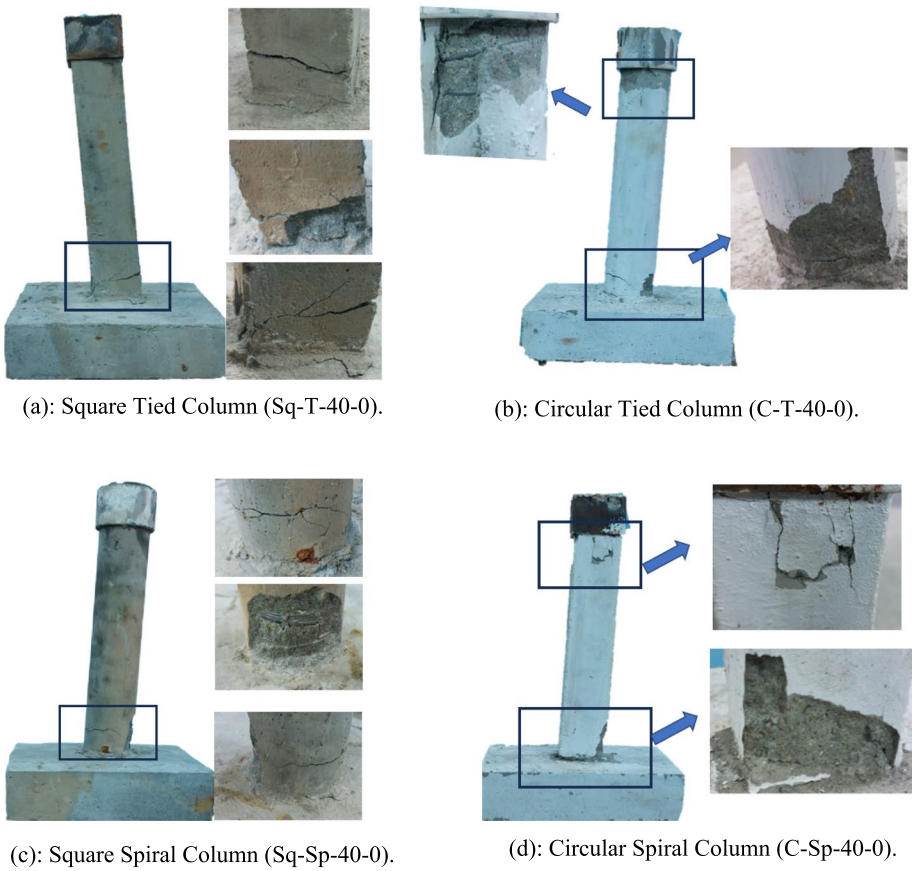

Fig. 13 The failure mode of Group 3 specimens**. a** Square tied column (Sq-T-40-0). **b** Circular tied column (C-T-40-0). **c** Square spiral column (Sq-Sp-40-0). **d** Circular spiral column (C-Sp-40-0)

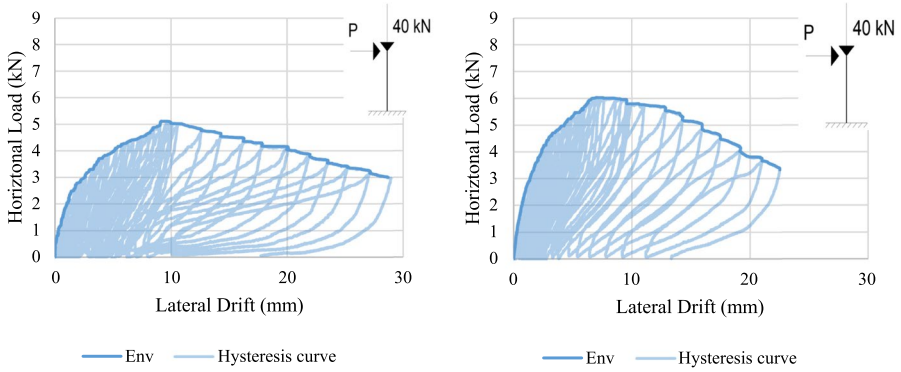

(a): The horizontal load-lateral drift curve for specimen (Sq-T-40-0).

(b): The horizontal load-lateral drift curve for specimen (C-T-40-0).

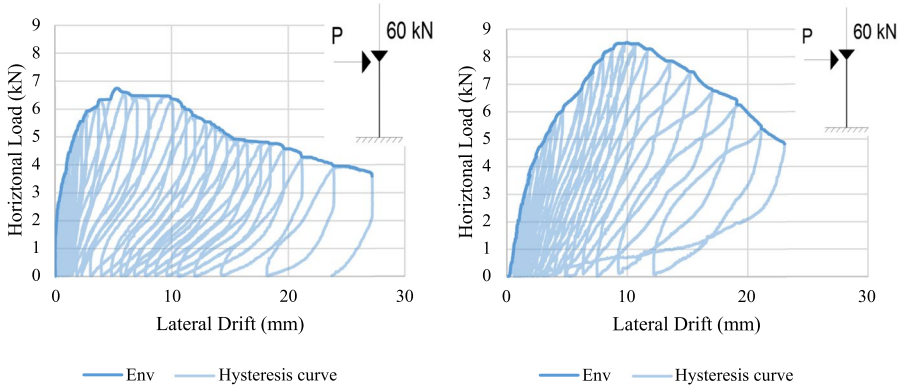

(c): The horizontal load-lateral drift curve for specimen (Sq-Sp-40-0).

(d): The horizontal load-lateral drift curve for specimen (C-Sp-40-0).

Fig. 14 The horizontal load-lateral drift curve for Group 3. **a** The horizontal load-lateral drift curve for specimen (Sq-T-40-0). **b** The horizontal load-lateral drift curve for specimen (C-T-40-0). **c** The horizontal load-lateral drift curve for specimen (Sq-Sp-40-0). **d** The horizontal load-lateral drift curve for specimen (C-Sp-40-0)

maximum lateral drift by 8.24%, suggesting reduced ductility despite the high strength gain. Notably, circular column with spirals increased maximum lateral drift by 16%. This seemingly counterintuitive result might be due to the combined effect of enhanced confinement offered by spirals and the inherent ductility of circular sections.

Analyzing the behavior of concrete columns with various shapes and reinforcement at a 25% corrosion level yielded intriguing results as illustrated in Fig. 21. While circular tied column displayed a substantial 11.6% increase in the absolute peak load compared to square and surprisingly exhibited a 15.4% higher maximum lateral drift, this suggested enhanced ductility despite strength gains. For spirals, the trend flipped: circular column unexpectedly lost 9.6% of the absolute horizontal peak load to square column but compensated with a significant 29% increase in maximum lateral drift, hinting at improved ductility despite the strength drop. Within cross-sectional shapes, spirals significantly enhanced load-carrying capacity, with square column and circular column increased the absolute horizontal peak load by 33.4% and 7.6% respectively. At the expense of ductility, as square column and circular column exhibited a decrease of 10.5% and 31.26% respectively.

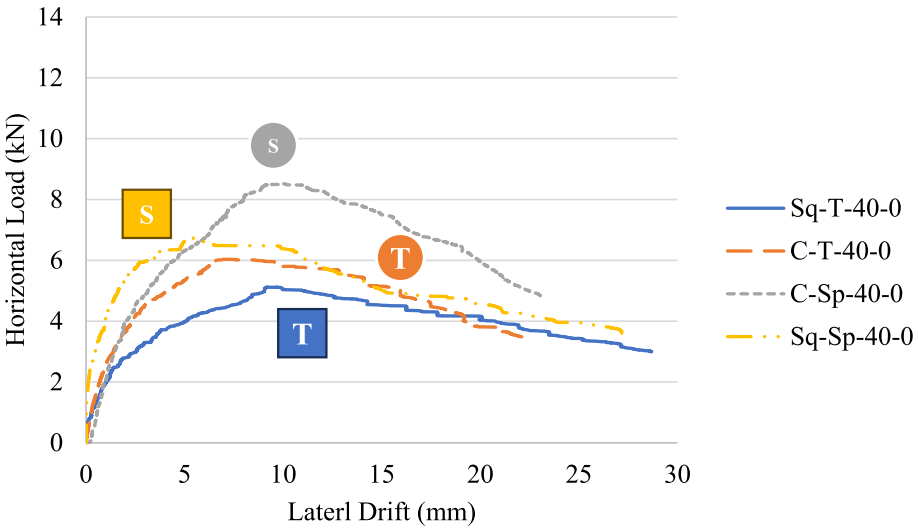

Fig. 15 Envelope curves for Group 3 specimens (control specimens)

Square tied column

Figure 22 shows the envelopes for square tied columns. Comparing Sq-T-95-0 and Sq-T-40-0 showed that increasing the axial load ratio from 40 to 95% in square tied columns dramatically enhanced lateral load-carrying capacity, with a 135.8% increase in absolute horizontal peak load. Interestingly, this gain in strength was accompanied by a decrease

Fig. 16 The failure mode of Group 4 specimens. **a** Square tied column (Sq-T-40-15). **b** Circular tied column (C-T-40-15). **c** Square spiral column (Sq-Sp-40-15). **d** Circular spiral column (C-Sp-40-15)

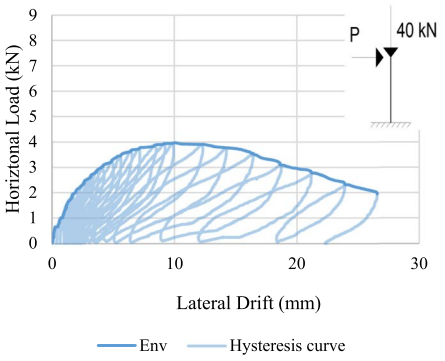

(a): The horizontal load-lateral drift curve for specimen (Sq-T-40-15).

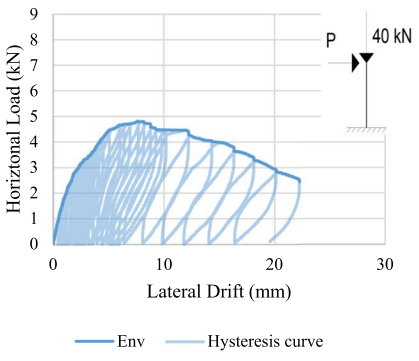

(b): The horizontal load-lateral drift curve for specimen (C-T-40-15).

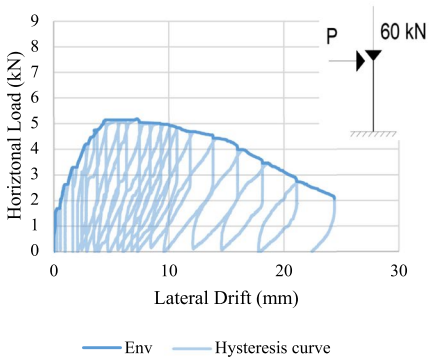

(c): The horizontal load-lateral drift curve for specimen (Sq-Sp-40-15).

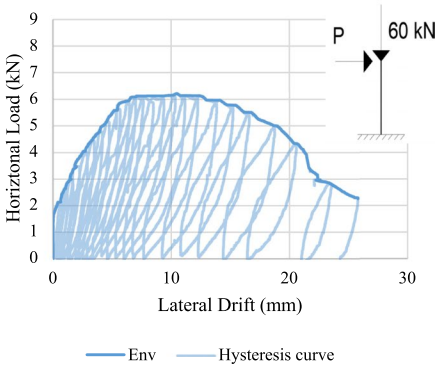

(d): The horizontal load-lateral drift curve for specimen (C-Sp-40-15).

Fig. 17 The horizontal load-lateral drift curve for Group 4. **a** The horizontal load-lateral drift curve for specimen (Sq-T-40-15). **b** The horizontal load-lateral drift curve for specimen (C-T-40-15). **c** The horizontal load-lateral drift curve for specimen (Sq-Sp-40-15). **d** The horizontal load-lateral drift curve for specimen (C-Sp-40-15)

in deformation, with a 47.7% reduction in maximum lateral drift. This highlights the significant impact of axial load on both strength and ductility. Moreover, introducing corrosion, however, produced detrimental effects. At both 15% and 25% corrosion levels, compared to non-corroded columns, the absolute horizontal peak load decreased. The decline was more pronounced at the higher corrosion level, with a 27.67% drop compared to 22.31% at corrosion level of 15%. Additionally, both corrosion levels led to a reduction in maximum lateral drift, less substantial than the strength reduction where it decreased by 7.4% and 37.5% for corrosion level of 15% and 25% respectively. These findings emphasize the detrimental influence of corrosion on the structural integrity of concrete columns, progressively weakening their load-carrying capacity and reducing their deformation capacity.

Circular tied column

Figure 23 shows the envelope curves for circular tied columns. Increasing the axial load ratio from 40 to 91% significantly affected the load-carrying capacity of circular tied columns. Compared to the high-load scenario, the absolute horizontal peak load at

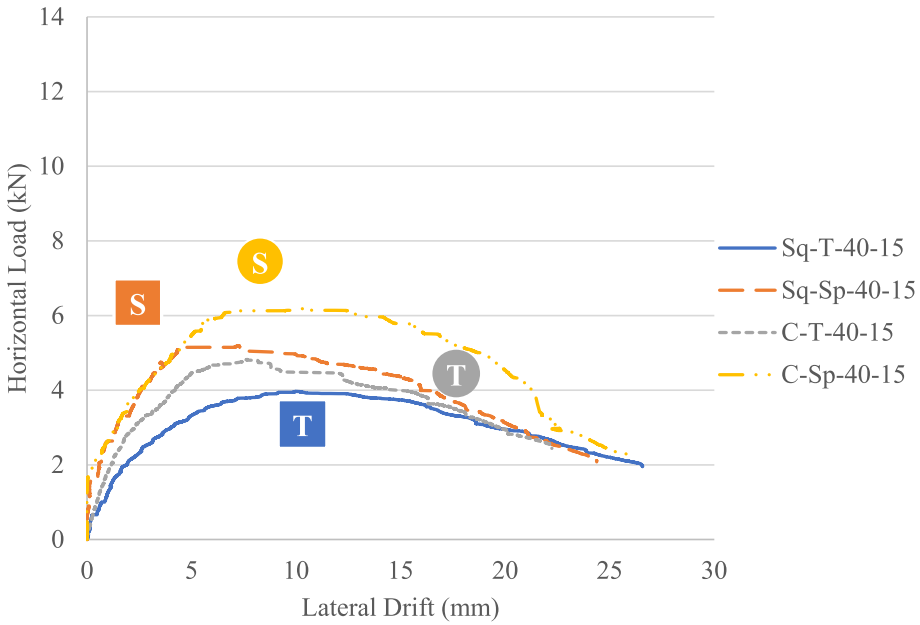

Fig. 18 Envelope curves for Group 4 specimens (15% corrosion level). **a** Square tied column (Sq-T-40-25). **b** Square tied column (C-T-40-25). **c** Square spiral column (Sq-Sp-40-25). **d** Circular spiral column (C-Sp-40-25)

the lower load ratio witnessed a substantial 72.7% increase. Interestingly, this strength gain came at the cost of reduced ductility, as evidenced by a 14.6% decrease in maximum lateral drift. These findings highlight the significant influence of axial load on both the strength and deformation characteristics of columns. Introducing corrosion, as expected, negatively impacted the structural integrity of circular tied columns. Investigating the effect of corrosion, at 15% corrosion level, the absolute horizontal peak load experienced a moderate 20% decrease, while the maximum lateral drift remained relatively unaffected with a slight 1.2% decrease. Meanwhile, at 25% corrosion level, the negative impact became more pronounced. The absolute horizontal peak load suffered a more substantial 30.55% reduction, and the maximum lateral drift displayed a more significant 8% decrease. These observations suggest that while initial corrosion levels might primarily affect strength, higher levels begin to impact ductility as well.

Square spiral column

Figure 24 shows the envelope curves for square spiral columns. To investigate the axial load ratio effect, comparison between Sq-Sp-81-0 and Sq-Sp-40-0 was conducted. It revealed that increasing the axial load ratio from 40 to 81% led to a substantial 41% increase in absolute horizontal peak load. However, this enhanced strength came at the cost of reduced ductility, as evidenced by a 37.6% decrease in maximum lateral drift. These findings further underline the strong influence of axial load ratio on the lateral load-carrying capacity and drift characteristics of square spiral columns. Furthermore, comparison among corroded and non-corroded specimens at 40% axial load ratio was conducted. It was found that corrosion, as expected, had a detrimental impact on column behavior. Both 15% and 25% corrosion levels resulted in reductions in absolute horizontal peak load compared to non-corroded columns. The decline was

(a): Square Tied Column (Sq-T-40-25).

(b): Square Tied Column (C-T-40-25).

(c): Square Spiral Column (Sq-Sp-40-25).

(d): Circular Spiral Column (C-Sp-40-25).

Fig. 19 The failure mode of Group 5 specimens. **a** The horizontal load-lateral drift curve for specimen (Sq-T-40-25). **b** The horizontal load-lateral drift curve for specimen (C-T-40-25). **c** The horizontal load-lateral drift curve for specimen (Sq-Sp-40-25). **d** The horizontal load-lateral drift curve for specimen (C-Sp-40-25)

more pronounced at the higher corrosion level, with a 26.82% drop compared to 23.3% at corrosion level of 15%. Interestingly, similar to the effect of axial load ratio, both corrosion levels also led to a reduction in maximum lateral drift, with a more significant decrease at the higher level (41% compared to 10.3%). This suggests that corrosion weakens columns not only by reducing their ability to resist loads but also by affecting their ductility as depicted in Fig. 24.

Circular spiral column

Due to premature failure under axial compressive load for specimen C-Sp-76-0 before the test commenced, direct comparison with C-Sp-40-0 is not entirely valid. While data from C-Sp-76-0 is limited, reducing the axial load ratio from 40 to 76% might result in lower load-carrying capacity and deformation capacity. Nevertheless, the observed 50.6% decrease in absolute horizontal peak load and 64.5% decrease in maximum lateral drift suggest significantly compromised structural integrity, likely due to the pre-test damage. Further investigation with additional specimens is needed to confirm this trend.

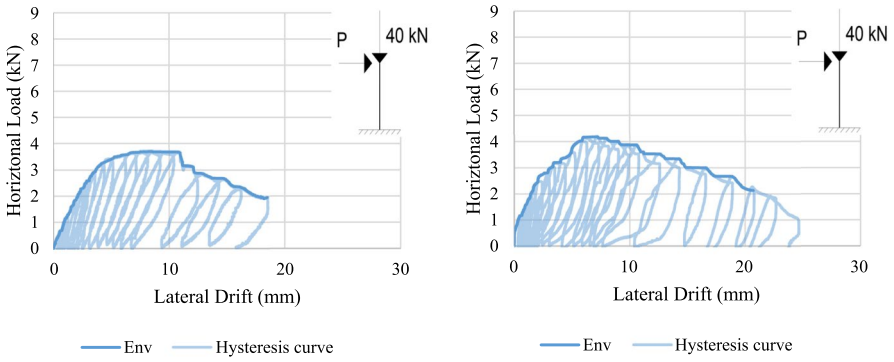

(a): The horizontal load-lateral drift curve for specimen (Sq-T-40-25).

(b): The horizontal load-lateral drift curve for specimen (C-T-40-25).

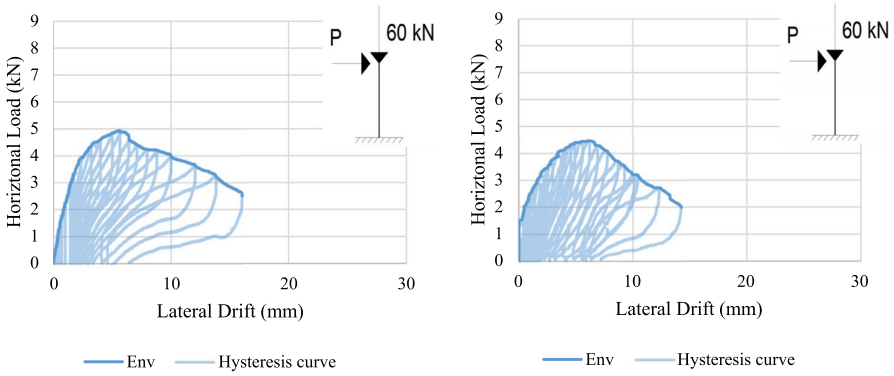

(c): The horizontal load-lateral drift curve for specimen (Sq-Sp-40-25).

(d): The horizontal load-lateral drift curve for specimen (C-Sp-40-25).

Fig. 20 The horizontal load-lateral drift curve for Group 5. **a** The horizontal load-lateral drift curve for specimen (Sq-T-40-25). **b** The horizontal load-lateral drift curve for specimen (C-T-40-25). **c** The horizontal load-lateral drift curve for specimen (Sq-Sp-40-25). **d** The horizontal load-lateral drift curve for specimen (C-Sp-40-25)

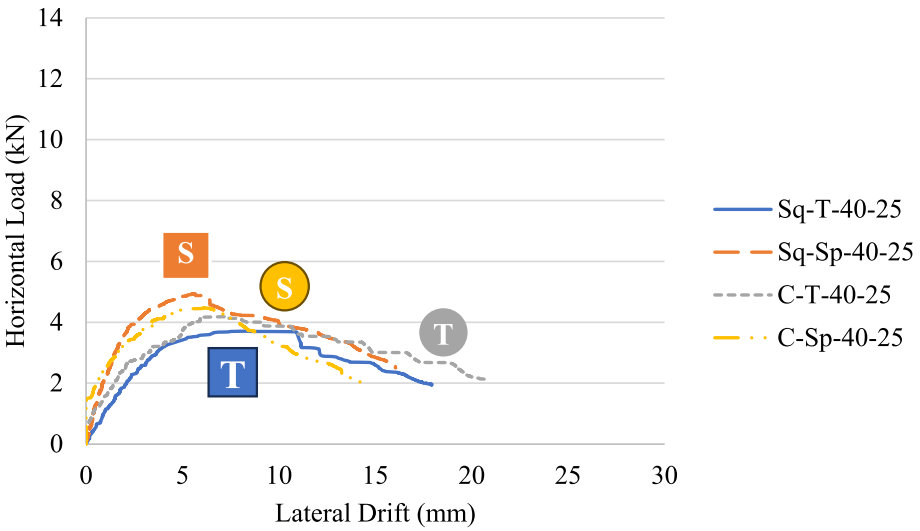

Fig. 21 Envelope curves for Group 5 specimens (25% corrosion level)

Table 6 Corroded specimens failure mode commentary

Group no	Commentary
Group 4	Investigation of failure modes exposed a prevalent pattern for most specimens—horizontal cracks on the loaded side and crushing on the opposing side (Fig. 16b, c, d), suggesting bending-dominant failure. Localized damage observed under the top encasement (Fig. 16a) can be attributed to stress concentrations stemming from its bearing failure prevention function**.** Visual inspection of the corroded specimens prior to test initiation revealed the presence of both red-brown rust staining and pre-existing cracking, indicative of advanced material degradation.
Group 5	Pre-test visual examination of corroded specimens revealed pronounced red-brown rust staining surpassing levels witnessed at 15% corrosion. Additionally, all specimens presented pre-existing cracks at the construction joint, attributable to the expansive nature of corrosion products. These cracks widened with increasing loading cycles in circular sections, as evident in Fig. 19b, d. Square sections, however, exhibited more extensive damage. Figure 19a illustrates the tied square column with a severely reduced steel cross-section and even breakage during loading. Figure 19c showcases the failure of the concrete cover in the spirally reinforced column, exposing pronounced deterioration within this zone, indicative of advanced material degradation across both reinforcement and surrounding concrete.

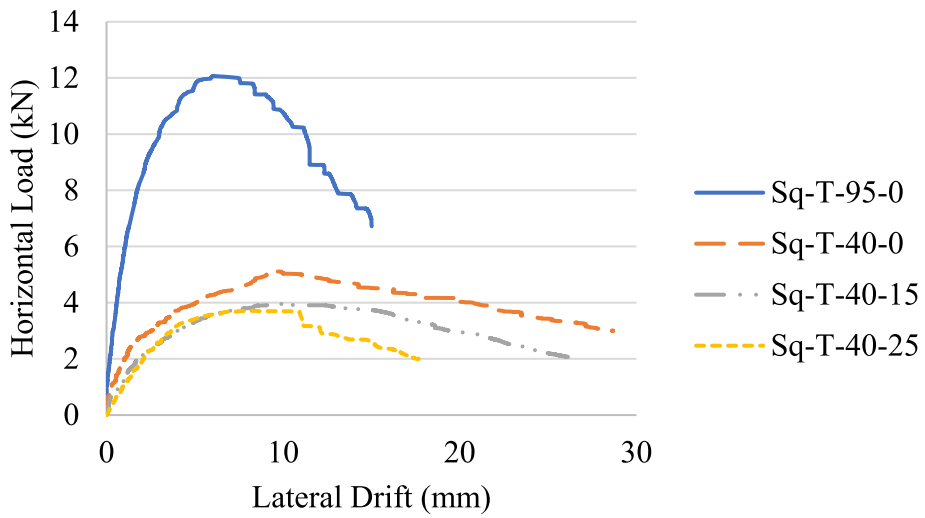

Fig. 22 Envelope curves for square tied columns

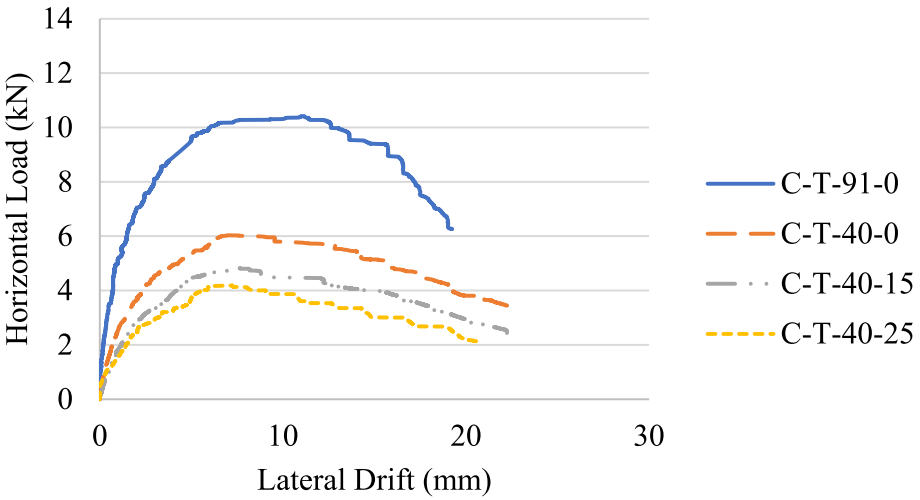

Fig. 23 Envelope curves for circular tied columns

Investigating corrosion effect, results revealed that corrosion had detrimental effects on strength but diverse effects on ductility. Whereas, at corrosion level of 15%, the absolute horizontal peak load decreased by 27.2%, indicating weakened load-bearing capability. However, surprisingly, the maximum lateral drift increased by 11.8%, suggesting potentially enhanced deformability at this corrosion level. Meanwhile, at corrosion level of 25%, the negative impact on strength intensified, with a 47.5% decrease in absolute horizontal peak load. In contrast, the maximum lateral drift decreased by 38.3%, indicating reduced ductility compared to the 15% corrosion level as shown in (Fig. 25).

Design charts

Normalized total dissipated energy

To enable fair comparison between different column types, the total dissipated energy of each specimen is normalized by dividing it by the total dissipated energy of the reference specimen, which in this case is the circular spiral column (C-Sp-40-0) as illustrated in (Fig. 26).

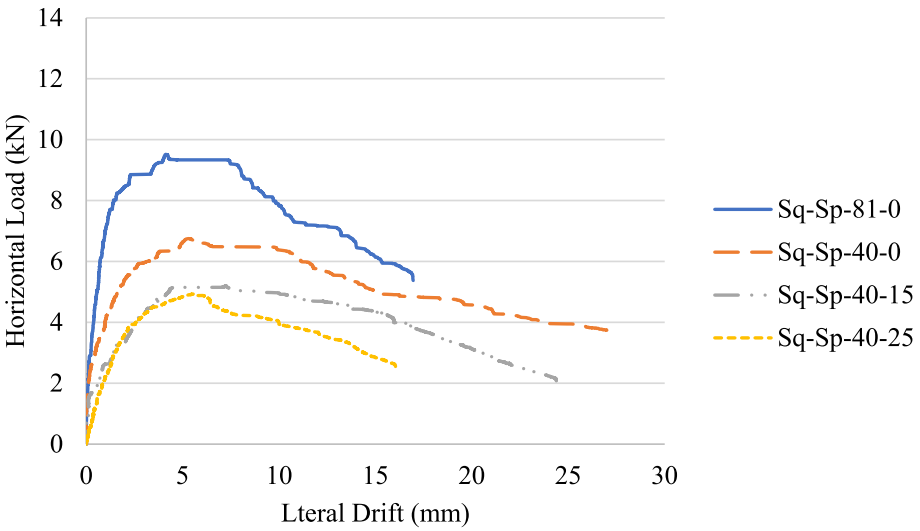

Fig. 24 Envelope curves for square spiral columns

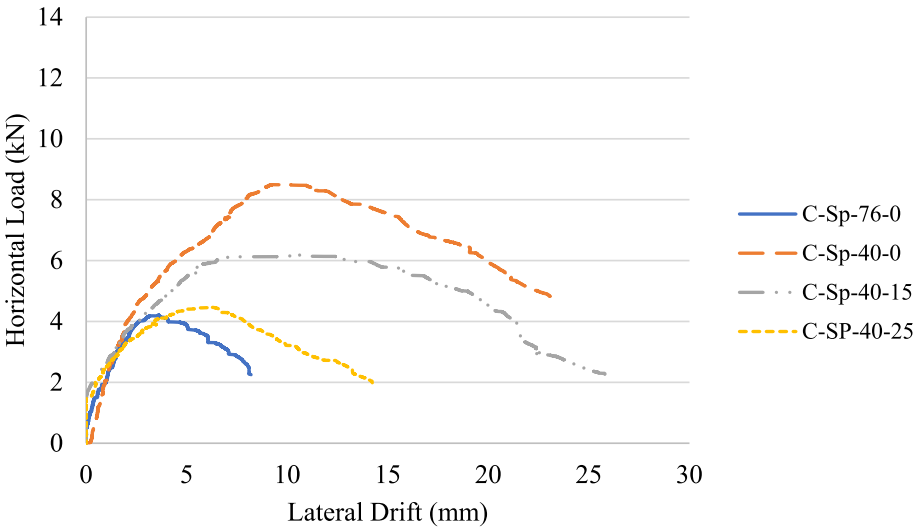

Fig. 25 Envelope curves for circular spiral columns

Figure 27 shows a clear downward trend, the more a concrete column is corroded, the less energy it can dissipate before breaking. This decline in energy absorption capacity can be predicted using the equations provided:

- For square tied column : $y = -0.0003x^2 - 0.01x + 0.7633 \quad R^2 = 1$
- For square spiral column : $y = -0.0002x^2 - 0.0162x + 0.9473 \quad R^2 = 1$
- For circular tied column : $y = -6E - 06x^2 - 0.0113x + 0.7262 \quad R^2 = 1$
- For circular spiral column : $y = -0.0016x^2 + 0.0131x + 1 \quad R^2 = 1$

Where:

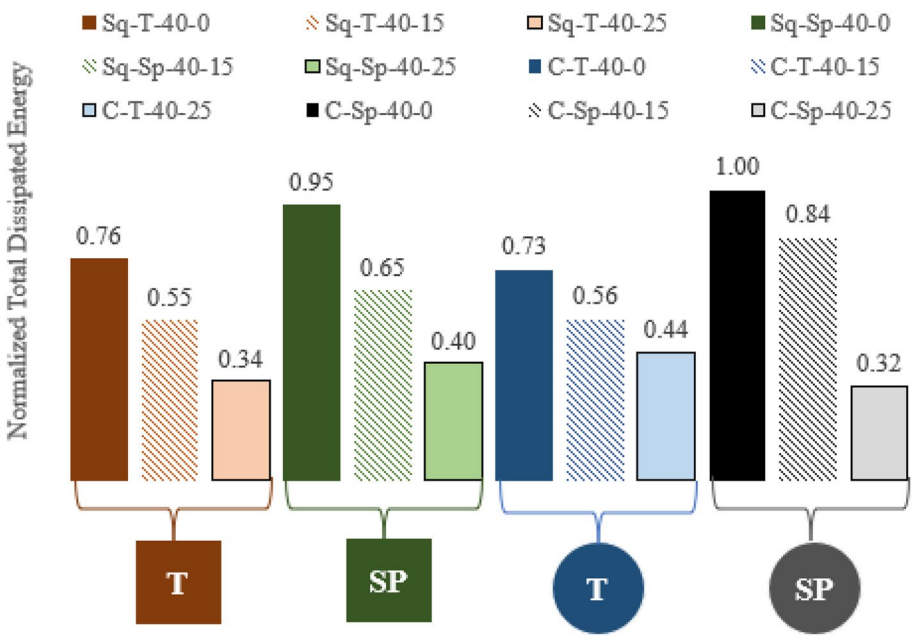

Fig. 26 Normalized total dissipated energy for specimen Groups 3–5

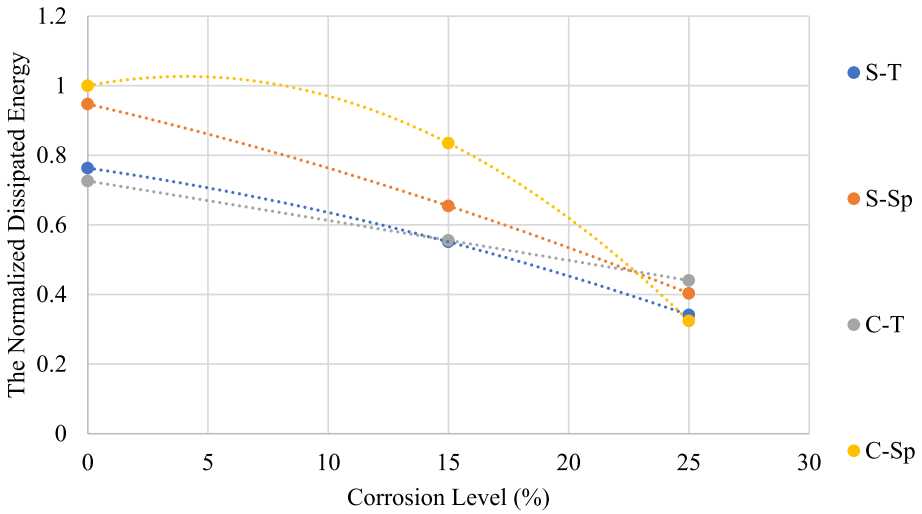

Fig. 27 Normalized total dissipated energy model

y: the normalized dissipated energy

x: the corrosion level %

R^2: mean squares represent an estimate of population variance

Normalized absolute peak load

Figure 28 visually depicts the inverse relationship between a concrete column's normalized absolute peak load and its corresponding level of corrosion (%). This normalized value is obtained by dividing the absolute peak load of each specimen by the value of absolute peak load for the non-corroded circular spiral reference specimen (C-Sp-40-0). Mathematically, the following equations can be used to predict this relationship:

■ For square tied column : $y = 0.0002x^2 - 0.0126x + 0.6002 \;\; R^2 = 1$

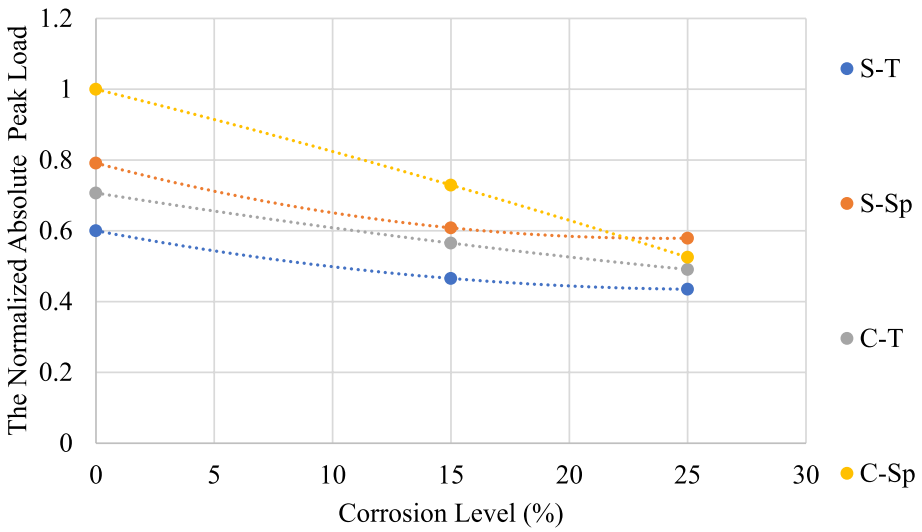

Fig. 28 The normalized absolute peak load

- For square spiral column : $y = 0.0004x^2 - 0.0177x + 0.7913 \ R^2 = 1$
- For circular tied column : $y = 8\text{E} - 05x2 - 0.0106x + 0.7069 \ R^2 = 1$
- For circular spiral column : $y = -9\text{E} - 05x^2 - 0.0166x + 1 \ R^2 = 1$

Where:

y: the normalized absolute peak load
x: the corrosion level %
R^2: mean squares represent an estimate of population variance

Conclusions

This research aims to investigate the interactions between cross-sectional shape, transverse reinforcement configuration, and corrosion degradation in reinforced concrete columns. Specific objectives include:

1. Quantifying the influence of cross-sectional shape on load-carrying capacity, ductility, and failure modes under various loading scenarios
2. Evaluating the effectiveness of ties versus spirals in enhancing column performance under combined axial and lateral varying drift
3. Assessing the impact of corrosion on the structural behavior of columns with different shapes and reinforcement types

After analyzing the findings of the aforementioned study, the following conclusions have been drawn:

(a) The implementation of spiral stirrups as transverse reinforcement significantly enhanced the axial load-carrying capacity of concrete columns subjected to compressive loading. Compared to separate ties stirrups, spirals improved the ultimate load capacity by 16.13% and 20% for square and circular sections, respectively. However, this reinforcement type also exhibited a contrasting effect on axial deformation, increasing the final shortening by 53.2% and 32% for square and circular columns, respectively.

(b) The load-carrying capacity of columns subjected to combined axial and horizontal loading conditions exhibits a complex interaction, while increasing the axial load ratio initially allows for higher horizontal loads, until reaching critical point where the axial load governs the failure mode.

(c) For non-corroded control columns, spiral reinforcement significantly improved the horizontal load-carrying capacity (32% for square column, 40.86% for circular column), but its impact on the maximum lateral drift differed: square column decreased by 5.27%, while circular column increased by 2.44%.

(d) For non-corroded control specimens, circular columns outperformed square columns in both tied and spiral reinforcement configurations. Compared to square column, circular tied column displayed 18% higher absolute horizontal peak load and 21.5% lower lateral drift, while circular spiral column achieved 26% higher absolute horizontal peak load and 15% lower lateral drift. These results highlight the advantages of circular columns in enhancing combined axial–lateral response due to improved geometrical efficiency and reduced stress concentrations.

(e) Across all column types, stirrups exhibit a higher tendency to corrosion compared to longitudinal reinforcement due to their smaller diameter. This reduced cross-sectional area translates to a higher current density per unit area under the same corrosion conditions, accelerating the deterioration process.

(f) While spiral stirrups provide enhanced mechanical properties, their continuous form presents a disadvantage in terms of corrosion resistance. The uninterrupted metallic path facilitates the passage of electrical current, accelerating the corrosion process compared to the separated configuration of tied stirrups.

(g) Across all column types, a rise in corrosion rate resulted in a reduction in the absolute horizontal peak load paired with an accelerated deterioration in overall performance.

(h) Circular spiral columns exhibited the most rapid degradation in performance due to corrosion, minimizing the benefits of the spiral reinforcement and revealing their behavior comparable to that of tied columns. This trend suggests an even more pronounced deterioration at higher corrosion levels.

(i) Both 15% and 25% corrosion levels resulted in reductions in absolute horizontal peak load and the maximum lateral drift compared to non-corroded columns.

Abbreviations

RFT	Steel reinforcement
M_{specimen}	Molar mass of reinforcing bars
m_{loss}	The required mass loss due to corrosion
n_{specimen}	The corroded material's valence (free electrons), equals to 2 for reinforcing steel
current	The induced current
C_{Faraday}	Faraday's constant
λ	Constant taking into consideration the likelihood that the corrosive process would not begin right away
f_{cu}	Concrete characteristic strength in MPa
f_y	Steel yield strength of longitudinal reinforcement in MPa
LVDT	Linear variable differential transducer

Acknowledgements
Not applicable

Authors' contributions
All authors read and approved the final manuscript.

Funding
Not applicable.

Availability of data and materials
The datasets used and/or analyzed during the current study are available from the corresponding author on reasonable request.

Declarations

Competing interests
The authors declare that they have no competing interests.

Received: 9 April 2024 Accepted: 30 June 2024
Published online: 17 July 2024

References

1. Austin SA, Lyons R, Ing MJ (2004) Electrochemical behavior of steel-reinforced concrete during accelerated corrosion testing. Corrosion 60(2):203–212. https://doi.org/10.5006/1.3287722
2. Meda A, Mostosi S, Rinaldi Z, Riva P (2014) Experimental evaluation of the corrosion influence on the cyclic behaviour of RC columns. Eng Struct 76:112–123. https://doi.org/10.1016/j.engstruct.2014.06.043

3. Li Q, Jin X, Yan D, Fu C, Xu J (2021) Study of wiring method on accelerated corrosion of steel bars in concrete. Constr Build Mater 269:121286. https://doi.org/10.1016/j.conbuildmat.2020.121286
4. Basdeki M, Koulouris K, Apostolopoulos C (2022) Effect of corrosion on the hysteretic behavior of steel reinforcing bars and corroded RC columns. Appl Sci 12(15):7451. https://doi.org/10.3390/app12157451
5. Li Q, Niu DT, Liu L (2012) The experimental study on reinforced concrete short-columns restrained by corroded stirrups. Adv Mater Res 446:1376–1379. https://doi.org/10.4028/www.scientific.net/AMR.446-449.1376
6. Mohammed AMY, Ahmed A, Maekawa K (2013) Seismic evaluation of RC columns considering equivalency of circular and square cross-sections. In: Proceedings of the Thirteenth East Asia-Pacific Conference on Structural Engineering and Construction (EASEC-13). The Thirteenth East Asia-Pacific Conference on Structural Engineering and Construction (EASEC-13), p D-1
7. Ahmed A, Mohammed AMY, Maekawa K (2014) Change of behaviour of circular and square columns with different amount of corrosion and reinforcement. In: Proceedings of the 10th fib International PhD Symposium in Civil Engineering. 10th International Federation for Structural Concrete (fib) International PhD Symposium in Civil Engineering 2014, p 523–528
8. Mohammed AMY, Ahmed A, Maekawa K (2019) Performance comparison of circular and square RC columns under monotonic loading conditions. KSCE J Civ Eng 23(1):210–216. https://doi.org/10.1007/s12205-018-0621-6
9. Mohammed AMY, Ahmed A, Maekawa K (2020) Comparative nonlinear behavior of corroded circular and square RC columns. KSCE J Civ Eng 24(7):2110–2119. https://doi.org/10.1007/s12205-020-1730-6
10. Ahmed A, Mohammed AMY, Maekawa K (2021) Correlation of high cycle fatigue behavior of circular and square reinforced concrete columns subjected to shear controlled cyclic loading. KSCE J Civ Eng 25(5):1755–1764. https://doi.org/10.1007/s12205-021-0850-y
11. Ahmed A, Mohammed AMY, Maekawa K (2021) Performance comparison of high strength reinforced concrete circular and square columns subjected to flexural controlled cyclic loading. Civ Eng J 7(1):83–97. https://doi.org/10.28991/cej-2021-03091639
12. Jabbour S, Martín-Pérez B (2010) Cover cracking in RC columns subjected to reinforcement corrosion under sustained load. Proceedings of FraMCoS-7, Seoul, Korea, p 23–28
13. Ma Y, Che Y, Gong J (2012) Behavior of corrosion damaged circular reinforced concrete columns under cyclic loading. Constr Build Mater 29:548–556. https://doi.org/10.1016/j.conbuildmat.2011.11.002
14. Radhi M, Hassan MS, Gorgis IN (2020) Compressive performance of corroded reinforced concrete columns. Eng Technol J 38(11):1618–1628. https://doi.org/10.30684/etj.v38i11a.1545
15. Jabbour S, Martín-Pérez B, Liu M (2022) Reinforcement corrosion of circular concrete columns under sustained load. In: MATEC Web of Conferences (Vol. 364). EDP Sciences, p. 02021. https://doi.org/10.1051/matecconf/202236402021
16. Mahmood LB, Lateef AM (2023) Effect of concrete type (normal concrete and high-performance concrete) on the corrosion degree of corroded circular-short columns. Math Stat Eng Appl 72(1):1037–1053. https://doi.org/10.17762/msea.v72i1.2114
17. Saeedi Razavi B, Goharrokhi A, Mobashery A (2023) The effect of transverse reinforcement corrosion on the axial bearing capacity of reinforced concrete columns. Adv Standards Appl Sci 1(3). https://doi.org/10.22034/ASAS.2023.384957.1020
18. Aminulai HO, Robinson AF, Ferguson NS, Kashani MM (2023) Nonlinear behaviour of corrosion damaged low-strength short reinforced concrete columns under compressive axial cyclic loading. Eng Struct 289:116245. https://doi.org/10.1016/J.ENGSTRUCT.2023.116245

Publisher's Note